Coherent dynamics of Rydberg atoms in cosmic-microwave-background radiation

Timur V. Tscherbul and Paul Brumer

Chemical Physics Theory Group, Department of Chemistry, and Center for Quantum Information and Quantum Control,
University of Toronto, Toronto, Ontario M5S 3H6, Canada

Rydberg atoms excited by cold blackbody radiation are shown to display long-lived quantum coherences on time scales of tens of picoseconds. By solving non-Markovian equations of motion with no free parameters we obtain the time evolution of the density matrix and demonstrate that the blackbody-induced temporal coherences manifest as slowly decaying (100 ps) quantum beats in time-resolved fluorescence. An analytic model shows the dependence of the coherent dynamics on the energy splitting between atomic eigenstates, transition dipole moments, and coherence time of the radiation. Experimental detection of the fluorescence signal from a trapped ensemble of 10^8 Rydberg atoms is discussed, but shown to be technically challenging at present, requiring cosmic-microwave-background amplification somewhat beyond current practice.

I. INTRODUCTION

The interactions of atoms and molecules with incoherent light (such as blackbody radiation, BBR) play a central role in research fields as diverse as photosynthesis [1–4], photovoltaics [5], precision spectroscopy and measurement [6], and atomic and molecular cooling and trapping [7,8]. Thermal BBR is a ubiquitous perturber that shifts atomic energy levels [10], limiting the accuracy of modern atomic clocks [6,9] and reducing the lifetime of Rydberg atoms [7,11–13] and trapped polar molecules [8]. Recent theoretical developments suggest, however, that quantum-noise-induced coherence effects induced by BBR can be used to cool quantum systems [14] and enhance the efficiency of solar cells [5].

The dynamical response of a material system to incoherent light is determined, among other factors, by the coherence time, a time scale over which the phase relationship between the different frequency components of the light source is maintained [15]. A natural light source such as the Sun is well characterized as a BBR emitter with a temperature of $T = 5.6 \times 10^3$ K and a extremely short coherence time of $\tau_c = \hbar/kT \sim 1.3$ fs [16–20], where k is the Boltzmann constant. As a consequence, incoherent excitation of atomic systems on time scales relatively long compared to τ_c produces stationary mixtures of atomic eigenstates that do not evolve in time [4,18,19,21]. However, the coherence time of BBR increases with decreasing temperature and can reach values in excess of 2 ps at 2.7 K, the temperature of the cosmic-microwave-background radiation (CMB) [22]. This motivates interest in examining the temporal dynamics of atomic systems interacting with the CMB. However, since the CMB intensity is $(300/2.7)^4 = 1.5 \times 10^8$ weaker than that of BBR at 300 K, the absorption signal in most ground-state atoms and molecules even with suitably amplified CMB radiation [23], is very small. As an initial step toward resolution of this difficulty, we propose to use highly excited Rydberg atoms, whose large transition dipole moments make them extremely sensitive to external field perturbations [7]. Previous experimental work has explored the absorption of BBR by Rydberg atoms, leading to population redistribution, photoionization, and lifetime shortening [7,11,13]. However, these experiments were focused on measuring population dynamics with no

attention to coherence effects. Similarly, no attention has been paid to coherence properties of the CMB and the role it might play in enhancing cosmological information (see, e.g., Refs. [24–27]).

In this article we examine long-lived quantum coherence effects that occur in one-photon absorption of cold blackbody radiation (CBBR—a term that we henceforth use to denote BBR at 2.7 K) by highly excited Rydberg atoms [7]. Using a non-Markovian approach [21,28] to explore the dynamics of one-photon CBBR absorption, we show that the time-dependent fluorescence intensities of Rydberg atoms exhibit the quantum beats due to the coherences induced by a suddenly turned-on interaction with CBBR. This suggests an experiment to explore the coherence properties of a cold trapped ensemble of Rb atoms in the presence of CBBR. Our results demonstrate that non-Markovian and quantum coherence effects play a major role in the short-time population dynamics induced by CBBR.

Furthermore, we develop an analytical model for the coherences in the long-time limit that is valid for an arbitrary noise source, here applied to CBBR. The model reproduces the coherent oscillations observed in numerical simulations of the density matrix and provides insight into the role of the energy level splittings, the transition dipole moments, and the coherence time of the radiation in determining the time evolution of the coherences. Significantly, we show that the ratio of coherences to populations declines with time as $1/|\omega_{ij}t|$, where ω_{ij} is the energy splitting between the eigenstates i and j. Thus, the physical origin of the long-lived coherences is due to the small energy splittings between the eigenstates populated by one-photon absorption of CBBR.

The paper is organized as follows. Section II discusses the theory and Sec. III provides results and a discussion of the nature of the development and depletion of the coherences.

II. THEORY

Theoretically, the interaction of BBR with atoms is usually considered within the framework of Markovian quantum optical master equations [29], leading to Pauli-type rate equations for state populations parametrized by the Einstein coefficients. These treatments generally assume that the coherences induced

by BBR are negligibly small. The non-Markovian approach adopted here [18,21,28] allows us to examine these noise-induced coherences and memory effects arising from a finite correlation time of BBR.

The time evolution of atomic populations and coherences under the influence of incoherent radiation (such as BBR), suddenly turned on at $t = 0$, is given by [20,21,28]

$$\rho_{ij}(t) = \frac{\langle \mu_{i0}\mu_{j0}^* \rangle_p}{\hbar^2} e^{-i\omega_{ij}t} \int_0^t d\tau' \int_0^t d\tau'' \mathcal{C}(\tau',\tau'') e^{i\omega_{i0}\tau'} e^{-i\omega_{j0}\tau''}. \tag{1}$$

Here $\rho_{ij}(t)$ are the elements of the atom density matrix in the energy representation, $\mu_{i0} = \langle 0|\hat{\mu}|i\rangle$ are the transition dipole moment matrix elements connecting the initial atomic eigenstate $|0\rangle = |n_0 l_0 m_0\rangle$ and the final states $|i\rangle = |nlm\rangle$ with energies ϵ_0 and ϵ_i, $\langle \cdots \rangle_p$ denotes the polarization-propagation average [30], and $\omega_{ij} = (\epsilon_i - \epsilon_j)/\hbar$. For the sake of clarity, we further assume that the atom resides in a single state $|0\rangle = |n_0 l_0 m_0\rangle$ before the BBR is turned on at $t = 0$. Since $\rho_{00} \simeq 1$ at all times, the density matrix [Eq. (1)] describes the populations and coherences among the states populated by BBR excluding the initial state [21].

The dynamics of the atom's response to incoherent radiation is determined by the two-time electric field correlation function $\mathcal{C}(\tau',\tau'') = \langle \mathcal{E}(\tau')\mathcal{E}^*(\tau'')\rangle$ in Eq. (1). For a stationary BBR source, the correlation function depends only on $\tau = \tau' - \tau''$ and is given by [16,17]

$$\mathcal{C}(\tau) = \mathcal{E}_0^2 (90/\pi^4)\zeta(4, 1 + i\lambda\tau), \tag{2}$$

where $\zeta(4,x)$ is the generalized Riemann ζ function [16,17], $\lambda = kT/\hbar$, T is the temperature of the BBR, and $\mathcal{E}_0^2 = [2\pi^3/(45\hbar^3 c^3)](kT)^4$ is the mean intensity of the BBR electric field [16,17,31]. Note that Eq. (2) applies when $\omega_{i0} > 0$ (absorption); $\mathcal{C}^*(\tau)$ should be used for stimulated emission ($\omega_{i0} < 0$). Because $\langle \mathcal{E}(\tau')\mathcal{E}(\tau'')\rangle = 0$ for CBBR [15,29], there is no coherence between those levels populated in absorption and those levels populated in stimulated emission from a given initial state [28]. Combining Eq. (2) with Eq. (1), and evaluating the time integrals, gives (see the Appendix for details)

$$\rho_{ii}(t) = \frac{\langle |\mu_{i0}|^2 \rangle_p}{\hbar^2} \{t[\mathcal{K}_0^{(+)}(\omega_{i0}, t) + \mathcal{K}_0^{(-)}(\omega_{i0}, t)] \\ - \mathcal{K}_1^{(+)}(\omega_{i0}, t) - \mathcal{K}_1^{(-)}(\omega_{i0}, t)\}, \tag{3}$$

where

$$\mathcal{K}_n^{(\pm)}(\omega, t) = \int_0^t \tau^n \mathcal{C}(\pm\tau)e^{\pm i\omega\tau}d\tau \tag{4}$$

are half-Fourier transforms of τ-scaled time correlation functions. In the long-time limit ($t \to \infty$), the right-hand side of Eq. (3) grows linearly with t. Note that since we neglect spontaneous emission, the long-time limit is restricted to time scales that are short compared to the (very long) radiative lifetime, 200 μs, of the $65s$ state [32]. Using an integral representation for the generalized Riemann ζ function, we

obtain the limit (see the Appendix for details)

$$\rho_{ii}(t) = \frac{2\pi}{\hbar^2}\langle |\mu_{i0}|^2 \rangle_p I(\omega_{i0})t \quad (t \to \infty), \tag{5}$$

where $I(\omega) = \frac{2\hbar^3}{\pi c^3}\frac{\omega^3}{e^{\hbar\omega/kT}-1}$ is proportional to Planck's spectral density of BBR [15]. Hence, in the long-time (Markovian) limit, this approach reduces to Fermi's golden rule [30] commonly used to calculate the rates of BBR-induced population transfer [7,32].

The off-diagonal elements of the density matrix are obtained in the Appendix as

$$\rho_{ij}(t) = \frac{\langle \mu_{i0}\mu_{j0}^* \rangle_p}{\hbar^2}\frac{1}{i\omega_{ij}}\{[\mathcal{K}_0^{(+)}(\omega_{j0}, t) + \mathcal{K}_0^{(-)}(\omega_{i0}, t)] \\ - e^{-i\omega_{ij}t}[\mathcal{K}_0^{(+)}(\omega_{i0}, t) + \mathcal{K}_0^{(-)}(\omega_{j0}, t)]\} \tag{6}$$

Note that due to the double half-Fourier transforms in Eq. (1), Eq. (6) is sensitive to frequency cross correlations in the CBBR.

III. RESULTS AND DISCUSSION

A. Quantum dynamics of Rydberg atoms in CBBR: Populations and Coherences

We now apply the approach developed in Sec. II to examine the effects of quantum coherence in CBBR excitation of high-n Rydberg atoms. In order to parametrize the equations of motion (1), the Rydberg energies and transition dipole moments for ^{85}Rb are calculated by solving the radial Schrödinger equation for the Rydberg electron using the Numerov method [7,28,33]. To verify the accuracy of our results, we calculated the spontaneous emission rates from the $30s$ Rydberg state to various final np states. These results agree with those reported in Ref. [32] to within <5%.

Figure 1(a) shows the proposed setup for examining CBBR-induced coherences. A highly excited Rydberg state of an alkali-metal atom (here we focus on the $65p$ state of ^{85}Rb) is created at $t = 0$ by, e.g., excitation from the ground $5s$ state [34]. The newly prepared Rydberg state immediately starts to interact with the 2.7 K CBBR background, establishing a coherent superposition of the neighboring ns and nd Rydberg states [11]. In order to map out the time evolution of Rydberg populations and coherences, Eq. (1) is parametrized by the accurate transition dipole moments of ^{85}Rb and by the CBBR correlation function given by Eq. (2).

The rapid turn-on of CBBR acts as a coherent perturbation, creating a Rydberg wave packet that evolves with time and then slowly decoheres. Figure 1(b) shows the Rydberg energy levels of ^{85}Rb superimposed on the CBBR spectrum at 2.7 K. While the spectral width of the radiation is broad enough to excite the Rydberg levels with principal quantum numbers $n = 35$–115, the transition dipole moments [Fig. 1(c)] decrease dramatically with increasing $\Delta n = n - n_0$, so most of the population transfer from the $65p$ state occurs to the neighboring Rydberg states with the largest transition dipole moments [see Fig. 1(c)] via one-photon absorption ($66s$, $64d$) and stimulated emission ($65s$, $63d$). For this reason, CBBR-induced photoionization occurs at a slow rate and can be neglected for $n_0 = 65$. Spontaneous emission from the $65p$ state is also neglected
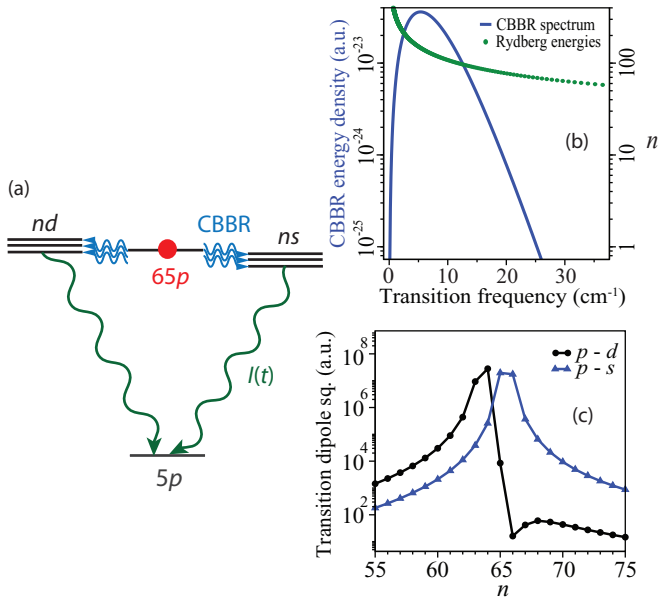
FIG. 1. (Color online) (a) Proposed experimental setup for observing long-lived quantum coherences with Rydberg atoms. At time $t = 0$, the atom in the $65p$ Rydberg state (red circle) begins to interact with CBBR (wavy lines), leading to a decohering Rydberg wave packet composed of the ns and nd states. The wave packet evolves and decays to the $5p$ state, with the quantum coherences leaving their signatures in the fluorescence signal $I(t)$ (see text). (b) Binding energies of highly excited ns Rydberg states of ^{85}Rb together with the 2.7 K Planck spectrum of CBBR radiation. The zero of energy corresponds to the ionization threshold. (c) n dependence of the calculated transition dipole moments squared from the initial $65p$ state to the ns states (triangles) and the nd states (circles).

since it occurs on a much longer time scale (200 μs [32]) than considered in this work.

Figure 2(a) shows the time evolution of several representative density matrix elements given by Eqs. (3) and (6). At $t \leqslant 50$ ps, the off-diagonal elements of the density matrix are of the same order of magnitude as the diagonal elements, suggesting the presence of coherences that play a role in the dynamical evolution of a Rydberg atom during the first 50 ps of its exposure to CBBR. At short times, state populations exhibit substantial deviations from the linear behavior predicted based on the standard Markovian quantum optical master equation [29]. The latter is shown in Fig. 2(a) as the linear solution $\rho_{ii}(t) = W_{0 \to i} t$, where $W_{0 \to i}$ is the standard BBR-induced transition rate related to the Einstein B coefficient [7]. The exact non-Markovian population dynamics is different in character and magnitude [28] but becomes linear in the larger t limit.

As shown in Fig. 2(a), the diagonal elements of the density matrix grow linearly with time while off-diagonal elements oscillate. As a result, the populations begin to significantly dominate over the coherences. Thus, BBR excitation produces a stationary mixture of atomic eigenstates, with coherences playing a negligible role in the long-time limit (nanoseconds) [18,20]. This gradual reduction of the coherences to population ratio is the mechanism of BBR-induced decoherence for the particular initial state. It differs
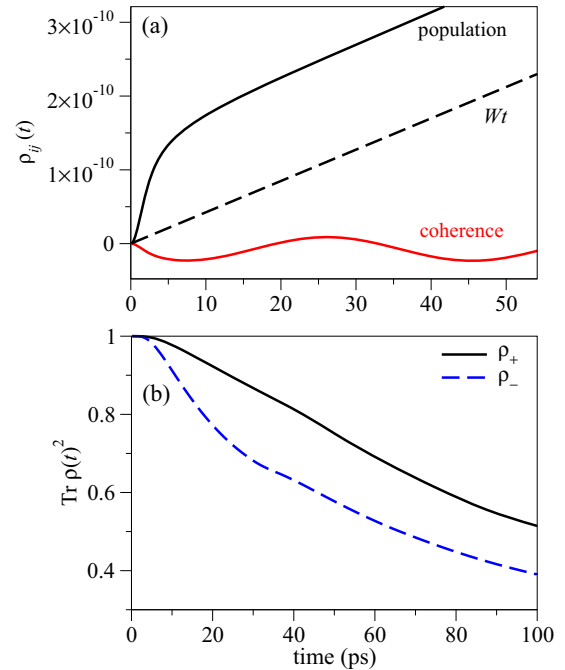

FIG. 2. (Color online) (a) The population of the representative $65s$ state of Rb as a function of time. (b) The time dependence of the purities for the absorption and stimulated emission blocks of the density matrix (7). The dashed line in the upper panel shows the expected Markovian behavior of the populations.

from other cases [35,36] where the initial state is a coherent superposition of energy eigenstates.

To see the decoherence times more clearly, Fig. 2(b) shows a useful measure of decoherence—the purity of the density matrix [37]

$$\varsigma = \text{Tr}\left(\rho_{\pm}^2\right) = [N_{\pm}(t)]^{-1} \sum_{i,j=1} |\langle i | \rho_{\pm}(t) | j \rangle|^2, \qquad (7)$$

where $\rho_{\pm}$ are the subblocks of the full density matrix composed of the states populated in absorption and stimulated emission from the initial state and the normalization factors $N_{\pm}(t) = \sum_i \langle i | \rho_{\pm}(t) | i \rangle^2$ ensure trace conservation [38]. The purity decays over a time scale of >100 ps, which signals the formation of an incoherent statistical mixture of atomic eigenstates in the process of CBBR excitation.

As is typical of direct CBBR measurements, the populations in Fig. 2(a) are quite small. As such, we note standard CMB amplification practices [23], which at present can give power gains in excess of 65 dB. Below we report results for a gain of 90 dB, which is technically possible, but experimentally challenging.

B. Observables: Time-resolved fluorescence

While clearly suggesting the existence of long-lived coherences on time scales of up to ~100 ps, neither the density matrix elements nor the purity values plotted in Fig. 2 are experimental observables. To explore the possibility of experimentally measuring the long-lived Rydberg coherences, we evaluate the time-resolved fluorescence signal from the ns and nd states of ^{85}Rb populated by the interaction with CBBR
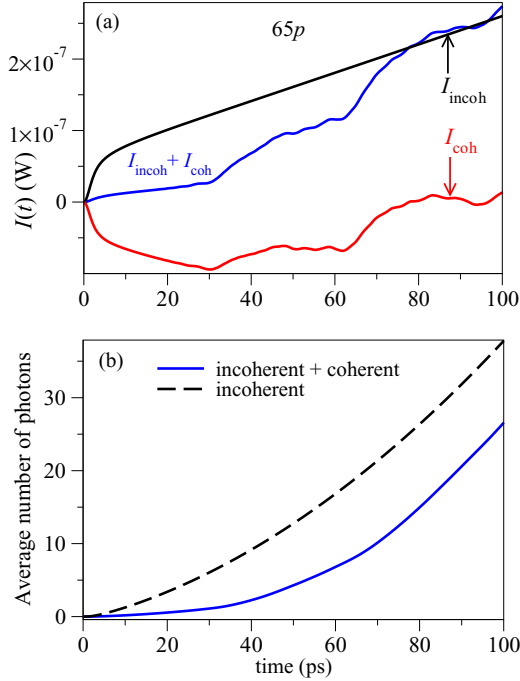
FIG. 3. (Color online) (a) Time-dependent fluorescence intensity for $N_a = 10^8$ Rydberg atoms initially in the $n_0 = 65p$ state interacting with CBBR amplified by a factor of 90 dB. (b) Average number of emitted photons $N_{ph}(t)$ (see text). The final state to which fluorescence occurs is $|i_f\rangle = |5p\rangle$. Also shown are the incoherent and coherent contributions to the total fluorescence intensity and to $N_{ph}(t)$.

(see Fig. 1). These states decay to the $5p$ state of Rb ($|i_f\rangle$) by emitting a photon at a transition frequency of 620 nm, which can be detected with high quantum efficiency. The total power emitted on these transitions by N_a atoms is given by [21,39]

$$I(t) = I_0 \text{Tr}\{|\hat{\mu} i_f\rangle\langle i_f \hat{\mu}|\rho(t)\} = I_0 \sum_{i,j=1} \mu_{ii_f}\mu_{i_f j}\rho_{ji}(t), \quad (8)$$

where $I_0 = N_a \frac{4}{3}\omega^4/(4\pi\epsilon_0 c^3)$, ϵ_0 is the vacuum permittivity, c is the speed of light, and ω is the transition frequency, assumed the same for all i and j states (since $|\omega_{ij}| \ll |\omega_{ii_f}|$).

Figure 3(a) shows the calculated time dependence of the fluorescence intensity for $N_a = 10^8$ Rb atoms interacting with amplified CBBR. The time-resolved emission signal displays pronounced oscillations over the timescales of 100 ps. The oscillations can be separated into coherent and incoherent parts, $I(t) = I_{incoh}(t) + I_{coh}(t)$, with [21]

$$I_{incoh}(t) = I_0 \sum_{i=1} \mu_{ii_f}\mu_{i_f i}\rho_{ii}(t),$$

$$I_{coh}(t) = I_0 \sum_{i \neq j} \mu_{ii_f}\mu_{i_f j}\rho_{ji}(t). \quad (9)$$

The incoherent contribution $I_{incoh}(t)$ depends on the diagonal elements of the density matrix (populations) while the coherent contribution $I_{coh}(t)$ specifically highlights the role of quantum coherences. As shown in Fig. 3(a), the coherent contribution to $I(t)$ remains significant up until $t < 100$ ps, suggesting the possibility of experimental observation of CBBR-induced Rydberg coherences and their subsequent decoherence.

Figure 3(b) displays the time dependence of the integrated fluorescence signal $F(t) = \int_0^t I(\tau)d\tau$, with $I(\tau)$ given by Eq. (8), which represents the experimentally measurable average number of photons emitted within the time window $[0,t]$: $N_{ph}(t) = F(t)/\hbar\omega$. The calculated photon flux is ~ 0.2 photons in the first 10 ps, ~ 2.3 photons in the first 40 ps, and ~ 26.6 photons in the first 100 ps of observation, assuming 100% photodetection quantum efficiency. While not showing any coherent oscillations, the integrated signal including the coherence contributions [solid line in Fig. 3(b)] is smaller than its incoherent counterpart [dashed line in Fig. 3(b)] by a factor of 4 at $t = 40$ ps and by 40% at $t = 100$ ps. This difference represents a clear signature of time evolution of the CBBR-induced coherences.

C. Analytics of noise-induced coherences and time scale for eigenstate formation

As shown in Figs. 2 and 3, the CBBR-induced coherent oscillations survive on a time scale much longer (~ 100 ps) than the coherence time of CBBR at 2.7 K ($\hbar/kT = 2.8$ ps). To explain this surprising longevity, we develop an analytical model for the time evolution of the coherences, based on Eq. (6). The model provides physical insight into the role of atomic energy levels, the transition dipole moments, and the coherence time of the radiation, as they determine the coherent evolution of the Rydberg atom. In particular, the results show coherences that oscillate with the frequency determined by the energy level splitting and coherence properties of the radiation that enter through the "phase shifts" and various prefactors that can be assumed to be constant in the long-time limit ($t \gg \tau_c$).

We emphasize that the results obtained here apply to the temporal dynamics of any atomic and/or molecular system coupled to incoherent radiation that is described by an arbitrary stationary correlation function, including CBBR.

Introducing the complex coefficients

$$\mathcal{S}_{ij}(t) = \mathcal{K}_0^{(+)}(\omega_{i0},t) + \mathcal{K}_0^{(-)}(\omega_{j0},t) \quad (10)$$

and using the property $\mathcal{S}_{ij}^* = \mathcal{S}_{ji}$ which follows from the definition (4), we can rewrite the off-diagonal density matrix elements [Eq. (6)] as

$$\rho_{ij}(t) = \frac{\langle \mu_{i0}\mu_{j0}^* \rangle_p}{\hbar^2} \frac{1}{i\omega_{ij}}[\mathcal{S}_{ij}^* - e^{-i\omega_{ij}t}\mathcal{S}_{ij}]. \quad (11)$$

The coefficients $\mathcal{S}_{ij}$ are plotted in Fig. 4 as a function of time for a sample pair of eigenstates $|1\rangle = |66s\rangle$ and $|2\rangle = |67s\rangle$ populated by interaction with CMB starting from the $|65p\rangle$ initial Rydberg state (see Fig. 1). The states are separated by an energy gap of $\hbar\omega_{21} = 0.86$ cm^{-1} ($1/\omega_{21} = 6.2$ ps). The correlation function $\mathcal{C}(\tau)$ of the BBR decays on the times cale $t_c \sim 3\tau_c \approx 10$ ps (see the Appendix). Accordingly, both the magnitudes and the phases of the coefficients $\mathcal{S}_{ij} = |\mathcal{S}_{ij}|e^{i\phi_{ij}}$ display time-dependent behavior during times $t < t_c$ (here ~ 10–15 ps), after which ($t > t_c$) they can be well approximated by a constant (the constant $\mathcal{S}_{ij}$ approximation, see Fig. 4). Note that the diagonal matrix elements $\mathcal{S}_{ii}$ are real.
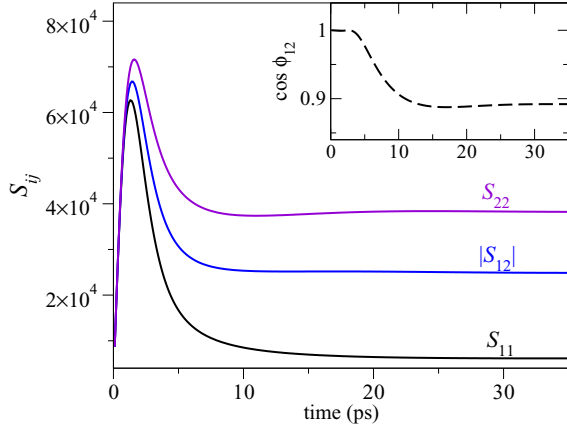
FIG. 4. (Color online) Time dependence of the coefficients $\mathcal{S}_{ij}$. The inset shows the cosine of the phase angle ϕ_{12} as a function of time. Note that the $\mathcal{S}_{ij}$ tend to constant values in the limit $t \gg \tau_c = 2.8$ ps as appropriate for the CMB.

For the absolute value of the off-diagonal density matrix elements in Eq. (11), we find

$$|\rho_{ij}(t)| = \frac{|\langle \mu_{i0} \mu_{j0}^* \rangle_p|}{\hbar^2} \frac{|\mathcal{S}_{ij}|}{|\omega_{ij}|} 2|\sin(\phi_{ij} - \omega_{ij}t/2)|, \quad (12)$$

whereas the real and imaginary parts of the coherences are given by

$$\text{Re}\,\rho_{ij}(t) = -\frac{\langle \mu_{i0} \mu_{j0}^* \rangle_p}{\hbar^2} \frac{|\mathcal{S}_{ij}|}{\omega_{ij}}[\sin(\phi_{ij} - \omega_{ij}t) + \sin\phi_{ij}],$$

$$\text{Im}\,\rho_{ij}(t) = \frac{\langle \mu_{i0} \mu_{j0}^* \rangle_p}{\hbar^2} \frac{|\mathcal{S}_{ij}|}{\omega_{ij}}[\cos(\phi_{ij} - \omega_{ij}t) - \cos\phi_{ij}]. \quad (13)$$

These expressions show that the absolute magnitude of the coherence oscillates with the frequency $\omega_{ij}/2$ determined by the energy splitting between the two eigenstates. The real and imaginary parts of the coherences oscillate at twice this frequency. A related result was obtained in Ref. [20] for the case of white noise. Equation (12) is, however, more general, as it applies to any kind of colored noise described by an arbitrary correlation function $C(\tau)$ (the only essential requirement being that the noise is stationary so that Eq. (6) applies). Each particular correlation function determines the dynamics through different $\mathcal{S}_{ij}$ coefficients in Eq. (11), which contains the characteristics of the radiation.

Equations (13) provide convenient analytic expressions for noise-induced coherences in the limit $t \gg \tau_c$ and are straight-forward to parametrize via the coefficients $\mathcal{S}_{ij}$. We note that these expressions could significantly reduce computational challenges in, e.g., calculating the density matrix dynamics of molecular systems. Figure 5(a) shows the real part of the coherence $\rho_{12}(t)$ calculated using Eq. (13) parametrized by the constant, asymptotic values for $|\mathcal{S}_{12}|$ and ϕ_{12} from Fig. 4. The analytic result is in excellent agreement with the exact calculation, thereby validating the constant $\mathcal{S}_{ij}$ approximation. The disagreement at short times is expected, since the $\mathcal{S}_{ij}$ vary strongly in this region, and hence cannot be approximated by constants. In particular, Eqs. (13) parametrized by the asymptotic values of $\mathcal{S}_{ij}$ disagree with the correct zero-time result $\rho_{ij}(0) = 0$. This drawback can be remedied, if desired,
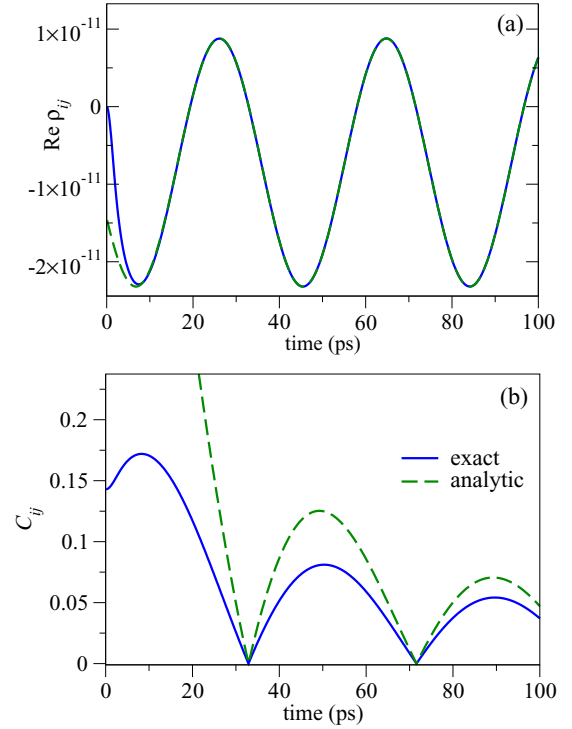

FIG. 5. (Color online) (a) The real part of the coherence between levels $|1\rangle = |66s\rangle$ and $|2\rangle = |67s\rangle$ as a function of time. Solid line, exact result [Eq. (5), Fig. 2]; dashed line, constant $\mathcal{S}_{ij}$ approximation (Eq. 13). (b) The ratio $\mathcal{C}_{12} = |\rho_{12}(t)|/[\rho_{11}(t) + \rho_{22}(t)]$ as a function of time. Solid line, exact result; dashed line, constant $\mathcal{S}_{12}$ approximation [Eq. (15)] .

by using a different parametrization such that $\mathcal{S}_{ij}(t) \to 0$ as $t \to 0$.

A useful measure of the relative importance of coherences and populations is the ratio [20]

$$\mathcal{C}_{ij}(t) = \frac{|\rho_{ij}(t)|}{\rho_{ii}(t) + \rho_{jj}(t)}. \quad (14)$$

A small value of $\mathcal{C}_{ij}$ indicates that the magnitude of the coherence ρ_{ij} is small compared to that of the populations, which is characteristic of a nearly pure statistical mixture. Hence, the time scale for the decay of $\mathcal{C}$ can be used to quantify the evolution from a purely coherent state at $t = 0$ to a statistical mixture of stationary eigenstates.

To obtain an analytic expression for the $\mathcal{C}$ ratio, we use an approximate result for state populations obtained from Eq. (3) by omitting the $\mathcal{K}_1^{(\pm)}$ terms, which are negligible compared to the other two terms in the limit $t \gg \tau_c$ [28]. Combining the resulting expression with Eq. (12), we find

$$\mathcal{C}_{ij}(t) = \frac{1}{|\omega_{ij}|t} \frac{|\langle \mu_{i0} \mu_{j0} \rangle_p|}{\langle |\mu_{i0}|^2 \rangle_p \mathcal{S}_{ii} + \langle |\mu_{j0}|^2 \rangle_p \mathcal{S}_{jj}} |\mathcal{S}_{ij}|$$
$$\times 2|\sin(\phi_{ij} - \omega_{ij}t/2)|. \quad (15)$$

Figure 5(b) plots the time variation of the $\mathcal{C}$ ratio for the Rydberg states $|1\rangle$ and $|2\rangle$ defined above. It is seen to decay in time as $1/(|\omega_{ij}|t)$ and oscillates with the frequency $\omega_{ij}/2$, due to the oscillating behavior of the absolute magnitude of the coherence (12). This shows that the coherences between

the Rydberg levels, evident in Figs. 2 and 3, survive for long times because of the small energy splittings between the levels populated by one-photon absorption and stimulated emission of CBBR. Longevity of coherences in association with small energy level splittings has been noted before, albeit in different contexts and with different functional dependences on the splittings [35,36,40] Indeed, in this case, the dependence on $\omega_{ij}t$ is reminiscent of the energy-time uncertainty principle, as the system strives, in time, to perceive individual energy levels.

IV. SUMMARY AND FUTURE PROSPECTS

In summary, the long-lived temporal coherence, and associated decoherence, in Rydberg atoms induced by the sudden turn-on of CBBR at 2.7 K has been examined. The physical mechanism behind the coherences and their slow decay is the long coherence time of CBBR and the small energy level splittings of the Rydberg levels excited by the CMB. The large transition dipole moments of the Rydberg atoms make these coherences manifest in various physical observables. Directly measuring CMB coherence properties via fluorescence detection would require 90-dB amplification of the incident CMB signal, beyond the current practice of 67 dB. At present, achieving such a high gain experimentally over a broad frequency interval (10–20 GHz) is a formidable challenge. However, recent developments in amplification technology allow for higher gains over much wider frequency intervals than possible with high electron mobility transistor (HEMT) amplifiers [41], and these may resolve experimental challenges associated with carrying out the proposed experiment.

Finally, we note that the long-lived coherences shown in Fig. 2 can also be observed with any experimental technique that is sensitive to coherent superpositions of the atom's excited states. Examples include selective field ionization [7], photoionization [7], and half-cycle pulse ionization [42]. The former technique also provides a direct route to measuring non-Markovian deviations from the linear behavior of state populations at short times (Fig. 2 a), which also relates to the coherence properties of CBBR [28].

One extension of this work is readily motivated. The study in this paper has examined the sudden turn-on associated with a single state prepared in an excited Rydberg state. However, slower preparation of Rydberg states, e.g., using a 15-ps laser pulse is expected to produce [34] additional interesting results. That is, such a pulse prepares a coherent superposition of five eigenstates centered around $n = 65$, rather than a single state, as assumed above. This superposition will then couple, via the CMB, to adjacent s and p Rydberg states. Fluorescence from this collection of levels is then expected to display a more complicated pattern of quantum beats than described above, which then decoheres in time. In addition, since the initial state is then a prepared superposition of energy eigenstates, decay of decoherence on assorted time scales is also anticipated [35,36]. Further, one can consider modifying the laser pulse shape in order to enhance the quantum beat signal. Such studies are under way.
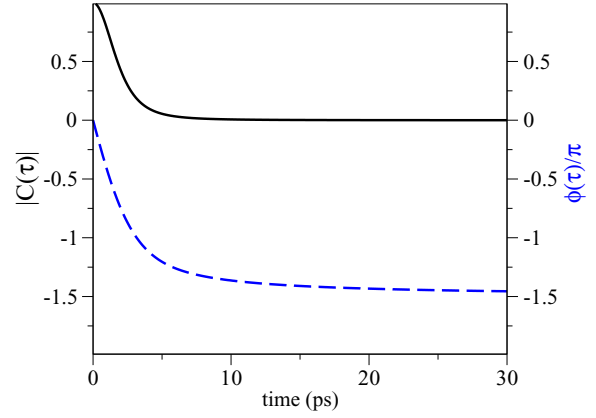
ACKNOWLEDGMENTS

FIG. 6. (Color online) Time dependence of CBBR correlation function $\mathcal{C}(\tau) = |\mathcal{C}(\tau)|e^{i\phi(\tau)}$ for $T = 2.718$ K (in units of $\mathcal{E}_0^2$, see Eq. (2) of the main text). Solid line, absolute magnitude ($|\mathcal{C}(\tau)|$); dashed line, phase ($\phi(\tau)/\pi$) [17].

APPENDIX

This appendix outlines the derivation of the equations of motion for the density matrix [Eqs. (3) and (5)] that describe the interaction of a Rydberg atom with BBR.

The time evolution of the density matrix for a Rydberg atom interacting with CBBR is given by Eq. (1). For a stationary CBBR source, the correlation function $\mathcal{C}(\tau', \tau'')$ is a function of $\tau = \tau' - \tau''$ only. The absolute value and the phase of the CBBR correlation function given by Eq. (2) are plotted in Fig. 6 as a function of τ for $T_{\mathrm{CMB}} = 2.718$ K [17].

By changing the integration variables $\tau_\pm = \tau' \pm \tau''$, Eq. (1) can be recast in the form

$$\rho_{ij}(t) = \frac{\langle \mu_{i0} \mu_{j0}^* \rangle_p}{\hbar^2} e^{-i\omega_{ij}t} \frac{1}{2} \left[\int_{-t}^{0} d\tau_- \int_{-\tau_-}^{\tau_-+2t} d\tau_+ f(\tau_+, \tau_-) \right.$$

$$\left. + \int_{0}^{t} d\tau_- \int_{\tau_-}^{2t-\tau_-} d\tau_+ f(\tau_+, \tau_-) \right], \quad \text{(A1)}$$

where $f(\tau_+, \tau_-) = \mathcal{C}(\tau_-) e^{i\omega_{i0}(\tau_++\tau_-)/2} e^{-i\omega_{j0}(\tau_+-\tau_-)/2}$. For $i = j$, the integrand simplifies to

$$f(\tau_-) = \mathcal{C}(\tau_-) e^{i\omega_{i0}\tau_-}, \quad \text{(A2)}$$

allowing the integration over τ_+ in Eq. (A1) to be performed analytically to yield the population dynamics

$$\rho_{ii}(t) = \frac{\langle |\mu_{i0}|^2 \rangle_p}{\hbar^2} \left[t\mathcal{I}_0(t) + \mathcal{I}_1(t) \right], \quad \text{(A3)}$$

with

$$\mathcal{I}_0(t) = \int_{-t}^{t} f(\tau_-) d\tau_-; \quad \text{(A4)}$$

$$\mathcal{I}_1(t) = \int_{-t}^{0} \tau_- [f(\tau_-) + f(-\tau_-)] d\tau_-. \quad \text{(A5)}$$

Splitting the range of integration in the first term on the right-hand side into positive and negative τ_- regions, relabeling the integration variable $\tau_- \to \tau$, and using Eq. (A2), we find

$$\mathcal{I}_0(t) = \int_0^t [\mathcal{C}(\tau)e^{i\omega_{i0}\tau} + \mathcal{C}(-\tau)e^{-i\omega_{i0}\tau}]d\tau \qquad (A6)$$

and

$$\mathcal{I}_1(t) = -\int_0^t \tau[\mathcal{C}(\tau)e^{i\omega_{i0}\tau} + \mathcal{C}(-\tau)e^{-i\omega_{i0}\tau}]d\tau. \qquad (A7)$$

Introducing the half-Fourier transforms

$$\mathcal{K}_0^{(\pm)}(\omega,t) = \int_0^t \mathcal{C}(\pm\tau)e^{\pm i\omega\tau}d\tau, \qquad (A8)$$

$$\mathcal{K}_1^{(\pm)}(\omega,t) = \int_0^t \tau\mathcal{C}(\pm\tau)e^{\pm i\omega\tau}d\tau, \qquad (A9)$$

we obtain Eq. (3) in the text.

In the case of $i \neq j$ (off-diagonal elements of the density matrix), the integrand depends on both τ_+ and τ_- via

$$f(\tau_+,\tau_-) = \mathcal{C}(\tau_-)e^{i\tau_+(\omega_{i0}-\omega_{j0})/2}e^{i\tau_-(\omega_{i0}+\omega_{j0})/2}. \qquad (A10)$$

Substituting Eq. (A10) in Eq. (A1) and evaluating the integral over τ_+ analytically (which is straightforward since $\mathcal{C}(\tau_-)$ is a function of τ_- only), we arrive at the result

$$\rho_{ij}(t) = \frac{\langle\mu_{i0}\mu_{j0}^*\rangle_p}{\hbar^2(i\omega_{ij})}\bigg\{\int_0^t [\mathcal{C}(\tau)e^{i\omega_{j0}\tau} + \mathcal{C}(-\tau)e^{-i\omega_{i0}\tau}]d\tau$$
$$- e^{-i\omega_{ij}t}\int_0^t [\mathcal{C}(\tau)e^{i\omega_{i0}\tau} + \mathcal{C}(-\tau)e^{-i\omega_{j0}\tau}]d\tau\bigg\}. \qquad (A11)$$

With the help of the definition (A8), we obtain Eq. (5) in the above text.

Using Eqs. (A3) and (A4) together with an integral representation for the generalized Riemann ζ function

$$\zeta(4,a) = \frac{1}{\Gamma(4)}\int_0^\infty \frac{x^3 e^{-ax}}{1-e^{-x}}dx, \qquad (A12)$$

where $\Gamma(x)$ is a Γ function, we get

$$\rho_{ii}(t \to \infty) = \frac{\langle|\mu_{i0}|^2\rangle_p}{\hbar^2}\int_{-\infty}^\infty \mathcal{C}(\tau)e^{i\omega_{i0}\tau}d\tau$$
$$= \mathcal{E}_0^2 \frac{90}{\pi^4\Gamma(4)}\int_0^\infty d\omega \frac{\omega^3 e^{-(1+i\lambda\tau)\omega}}{1-e^{-\omega}}$$
$$\times \int_{-\infty}^\infty d\tau e^{-i\lambda\tau\omega}e^{i\omega_{i0}\tau}. \qquad (A13)$$

The integral over τ is readily evaluated in terms of the Dirac δ function [$\int_{-\infty}^\infty e^{-i(\lambda\omega-\omega_{i0})\tau}d\tau = 2\pi\delta(\lambda\omega - \omega_{i0})$], and Eq. (A13) reduces to the Fermi golden rule result given by Eq. (4) in the text ($\lambda = kT/\hbar$):

$$\rho_{ii}(t \to \infty) = \mathcal{E}_0^2 \langle|\mu_{i0}|^2\rangle_p \frac{90}{\pi^4}\frac{2\pi}{\Gamma(4)}\frac{1}{\lambda^4}\frac{\omega_{i0}^3}{e^{\omega_{i0}/\lambda}-1}t$$
$$= \frac{4\langle|\mu_{i0}|^2\rangle_p}{3\hbar c^3}\frac{\omega_{i0}^3}{e^{\hbar\omega_{i0}/kT}-1}t. \qquad (A14)$$

Note that the proportionality coefficient in the second line of Eq. (A14) is the BBR-induced transition rate $W_{0\to i}$.

---

[1] G. S. Engel, T. R. Calhoun, E. L. Read, T.-K. Ahn, T. Mancal, Y.-C. Cheng, R. E. Blankenship, and G. R. Fleming, Nature (London) **446**, 782 (2007).

[2] E. Collini, C. Y. Wong, K. E. Wilk, P. M. G. Curmi, P. Brumer, and G. D. Scholes, Nature (London) **463**, 644 (2010).

[3] G. D. Scholes, J. Phys. Chem. Lett. **1**, 2 (2010).

[4] P. Brumer and M. Shapiro, Proc. Natl. Acad. Sci. U.S.A. **109**, 19575 (2012).

[5] M. O. Scully, K. R. Chapin, K. E. Dorfman, M. B. Kim, and A. Svidzinsky, Proc. Natl. Acad. Sci. U.S.A. **108**, 15097 (2011).

[6] T. Middelmann, S. Falke, C. Lisdat, and U. Sterr, Phys. Rev. Lett. **109**, 263004 (2012); M. S. Safronova, S. G. Porsev, U. I. Safronova, M. G. Kozlov, and C. W. Clark, Phys. Rev. A **87**, 012509 (2013).

[7] T. F. Gallagher, *Rydberg Atoms* (Cambridge University Press, Cambridge, UK, 1994).

[8] S. Hoekstra, J. J. Gilijamse, B. Sartakov, N. Vanhaecke, L. Scharfenberg, S. Y. T. van de Meerakker, and G. Meijer, Phys. Rev. Lett. **98**, 133001 (2007).

[9] V. D. Ovsiannikov, A. Derevianko, and K. Gibble, Phys. Rev. Lett. **107**, 093003 (2011).

[10] J. W. Farley and W. H. Wing, Phys. Rev. A **23**, 2397 (1981); L. Hollberg and J. L. Hall, Phys. Rev. Lett. **53**, 230 (1984); T. Nakajima, P. Lambropoulos, and H. Walther, Phys. Rev. A **56**, 5100 (1997).

[11] W. P. Spencer, A. G. Vaidyanathan, D. Kleppner, and T. W. Ducas, Phys. Rev. A **25**, 380 (1982); J. M. Raimond, P. Goy, M. Gross, C. Fabre, and S. Haroche, Phys. Rev. Lett. **49**, 117 (1982).

[12] M. Tada, Y. Kishimoto, K. Kominato, M. Shibata *et al.*, Phys. Lett. A **349**, 488 (2006).

[13] R. G. Hulet, E. S. Hilfer, and D. Kleppner, Phys. Rev. Lett. **55**, 2137 (1985).

[14] A. Mari and J. Eisert, Phys. Rev. Lett. **108**, 120602 (2012); B. Cleuren, B. Rutten, and C. Van den Broeck, *ibid.* **108**, 120603 (2012).

[15] L. Mandel and E. Wolf, *Optical Coherence and Quantum Optics* (Cambridge University Press, Cambridge, UK, 1995), Chap. 13.

[16] C. L. Mehta and E. Wolf, Phys. Rev. **134**, A1143 (1964); **134**, A1149 (1964).

[17] Y. Kano and E. Wolf, Proc. Phys. Soc. **80**, 1273 (1962).

[18] L. A. Pachón and P. Brumer, Phys. Rev. A **87**, 022106 (2013).

[19] K. Hoki and P. Brumer, Procedia Chem. **3**, 122 (2011).

[20] Z. Sadeq, M. Sc. thesis, University of Toronto, 2012; Z. Sadeq and P. Brumer (unpublished).

[21] X.-P. Jiang and P. Brumer, J. Chem. Phys. **94**, 5833 (1991); Chem. Phys. Lett. **180**, 222 (1991).

[22] P. D. Naselsky, D. I. Novikov, and I. D. Novikov, *The Physics of the Cosmic Microwave Background* (Cambridge University Press, Cambridge, UK, 2006).

[23] Coherent HEMT amplifiers are capable of large gains in the 20 GHz region of interest. See, e.g., Table 3 of N. Jarosik *et al.*, Astrophys. J. Suppl. Series **145**, 413 (2003), which describes the WMAP CMB amplification system consisting of two amplifiers, one radiatively cooled and the other at room temperature. As clarified by M. Pospieszalski in a private communication, the total gain of the two-amplifier chain is ∼67 dB.

[24] S. Weinberg, *Cosmology* (Oxford University Press, Oxford, 2008).

[25] G. Hinshaw *et al.*, Astrophys. J. Suppl. Ser. **180**, 225 (2009); E. Komatsu *et al.*, *ibid.* **180**, 330 (2009).

[26] R. Amanullah *et al.*, Astrophys. J. **716**, 712 (2010).

[27] R. Hakim, Ann. Phys. (Paris) **4**, 217 (1979).

[28] T. V. Tscherbul, L. A. Pachón, and P. Brumer (unpublished).

[29] H.-P. Breuer and F. Petruccione, *The Theory of Open Quantum Systems* (Clarendon Press, Oxford, 2006), Chap. 3.4.

[30] D. J. Griffiths, *Introduction to Quantum Mechanics* (Prentice Hall, Englewood Cliffs, NJ, 1995), Chap. 9.2.

[31] W. M. Itano, L. L. Lewis, and D. J. Wineland, Phys. Rev. A **25**, 1233 (1982).

[32] I. I. Beterov, I. I. Ryabtsev, D. B. Tretyakov, and V. M. Entin, Phys. Rev. A **79**, 052504 (2009); **80**, 059902(E) (2009).

[33] M. L. Zimmerman, M. G. Littman, M. M. Kash, and D. Kleppner, Phys. Rev. A **20**, 2251 (1979).

[34] J. A. Yeazell, M. Mallalieu, and C. R. Stroud, Jr., Phys. Rev. Lett. **64**, 2007 (1990); T. F. Gallagher, Phys. Scr. **76**, C145 (2007).

[35] Y. Elran and P. Brumer, J. Chem. Phys. **121**, 2673 (2004).

[36] Y. Elran and P. Brumer, J. Chem. Phys. **138**, 234308 (2013).

[37] M. Schlosshauer, *Decoherence and the Quantum-to-Classical Transition* (Springer-Verlag, Berlin, 2008), Chap. 2.4.

[38] T. A. Grinev and P. Brumer (to be published).

[39] W. Demtröder, *Atoms, Molecules and Photons*, 2nd ed. (Springer-Verlag, Berlin, 2010), Chap. 7.

[40] L. A. Pachón and P. Brumer, J. Phys. Chem. Lett. **2**, 2728 (2011).

[41] B. H. Eom, P. K. Day, H. G. LeDuc, and J. Zmuidzinas, Nat. Phys. **8**, 623 (2012).

[42] R. R. Jones, Phys. Rev. Lett. **76**, 3927 (1996).